http://dx.doi.org/10.7566/JPSJ.82.124604

Strong Quadrupole-Strain Interaction of Vacancy Orbital in Boron-Doped Czochralski Silicon

Kazuki OKABE[1,2], Mitsuhiro AKATSU[1,3], Shotaro BABA[1], Keisuke MITSUMOTO[1,4], Yuichi NEMOTO[1], Hiroshi YAMADA-KANETA[5], Terutaka GOTO[1*], Hiroyuki SAITO[2], Kazuhiko KASHIMA[1,2], and Yoshihiko SAITO[1,6]

[1]*Graduate School of Science and Technology, Niigata University, Niigata 950-2181, Japan*
[2]*GlobalWafers Japan Co., Ltd., Seirou, Niigata 957-0197, Japan*
[3]*Dresden High Magnetic Field Laboratory, Helmholtz-Zentrum Dresden-Rossendorf, D-01328 Dresden, Germany*
[4]*Max Planck Institute for Chemical Physics of Solids, D-01187 Dresden, Germany*
[5]*Department of Electrical Engineering and Electronics, Kyushu Institute of Technology, Kitakyushu 804-8550, Japan*
[6]*Toshiba Corporation, Yokohama 225-8522, Japan*

(Received May 14, 2013; accepted September 11, 2013; published online November 13, 2013)

We have carried out ultrasonic measurements of a boron-doped silicon ingot grown by the Czochralski method in order to determine the quadrupole-strain interaction constant of a vacancy orbital. The low-temperature softening of the elastic constant C_{44} shows a remarkable variation depending on positions of the ingot, which reflects the distribution of vacancy concentration N in the ingot. An infrared laser scattering tomograph was employed to measure the density and size of voids in the silicon wafers by determining the vacancy concentration N_{cons} consumed in void formation. Using a combination of laser scattering tomography and low-temperature softening, we have found a sum rule in which the initially created vacancy concentration N_{total} corresponds to the sum of the residual vacancy concentration N and the consumed vacancy concentration N_{cons} as $N_{\mathrm{total}} = N + N_{\mathrm{cons}}$. Taking account of the sum rule, we deduce the interaction constant $g_{\Gamma_5} = (2.8 \pm 0.2) \times 10^5$ K for the quadrupole-strain interaction $H_{\mathrm{QS}} = -g_{\Gamma_5} O_{zx} \varepsilon_{zx}$ of the vacancy orbital. The huge deformation energy of 1.6×10^5 K per vacancy with the Γ_8 ground state for unit strain $\varepsilon_{zx} = 1$ verified the strong electron–lattice interaction of the vacancy orbital. Employing the one-to-one correspondence between the softening of $\Delta C_{44}/C_{44} = 1.0 \times 10^{-4}$ down to 30 mK and the vacancy concentration of $N = 1.5 \times 10^{13}$ cm^{-3}, we can determine the vacancy concentration by low-temperature ultrasonic measurements. The present work surely puts forward a novel semiconductor technology based on low-temperature ultrasonic measurements for evaluating vacancy concentration in silicon wafers.

KEYWORDS: vacancy, boron-doped silicon wafer, ultrasound, quadrupole, softening

1. Introduction

There is an increasing demand for high-quality silicon wafers, which is responsible for high-density complementary metal oxide semiconductor (CMOS) devices in the next-generation standard beyond 19 nm in the process rule.[1)] For this purpose, precise control of bulk microdefect (BMD) corresponding to oxide precipitations as well as crystal-originated particle (COP) denoting voids is necessary.[2–5)] The vacancy corresponds to a lack of silicon atom from a lattice. The vacancies govern the BMD precipitation in device manufacturing processes and COP formation in crystal growth. The evaluation of vacancy concentration in silicon wafers, therefore, is crucial for pursuing better semiconductor device production. In our previous works, we successfully observed vacancy orbitals in silicon using low-temperature ultrasonic measurements.[6–8)] However, the determination of the interaction strength of vacancy orbitals with ultrasonic waves remains to be carried out.

Boron-doped silicon wafers are widely used for producing semiconductor devices. A vacancy orbital consisting of sp^3 dangling bonds ϕ_i with $i = 1, 2, 3$, and 4 around a vacant site with a cubic T_d symmetry splits into a singlet a_1 state and a triplet t_2 state owing to the transfer energy of $-\gamma = \langle \phi_j | H_0 | \phi_i \rangle$ $(i \neq j)$.[9)] The level scheme of a vacancy orbital is illustrated in Fig. 1. The vacancy orbital of the boron-doped silicon wafer possesses a positively charged state V^+ due to the charge neutrality between the vacancy releasing an electron and the boron dopant accepting an electron. An electron pair with antiparallel spin orientation occupies the singlet a_1 state and an electron is accommodated in one of the triplet t_2 state. The singlet a_1 state is located beneath the top of the valence band and the triplet t_2 state is located near the chemical potential. The spin–orbit interaction $H_{\mathrm{SO}} = \lambda \boldsymbol{L} \cdot \boldsymbol{S}$ $(\lambda < 0)$ for the electron in the triplet t_2 state with spin $S = 1/2$ and orbital angular momentum $L = 1$ brings about the Γ_8 quartet ground state and Γ_7 excited state.[7,8,10)] The electric quadrupole O_{zx} of the vacancy orbital consisting of the Γ_8 ground state couples to the elastic strain ε_{zx} associated with the transverse ultrasonic wave. The quadrupole-strain interaction of the vacancy orbital is also shown in Fig. 1. The low-temperature softening in the elastic constant of the boron-doped silicon wafer is described in terms of the quadrupole susceptibility of $-\chi$ proportional to the reciprocal temperature as $-\chi \propto 1/T$ due to the orbital degeneracy in the Γ_8 ground state.

Because the vacancy orbital has a spreading radius of up to 1 nm, the interaction of the electric quadrupole with the elastic strain is expected to be considerably enhanced.[11–13)] This significant property of the vacancy orbital brings about the successful observation of vacancies even at a very low concentration in the boron-doped silicon wafer currently used in the semiconductor industry. The accurate determination of the quadrupole-strain interaction constant is required for the numerical estimation of the vacancy concentration in the silicon wafer. In spite of many efforts for the investigation of low-temperature softening in boron-doped silicon, the experimental determination of the

©2013 The Physical Society of Japan

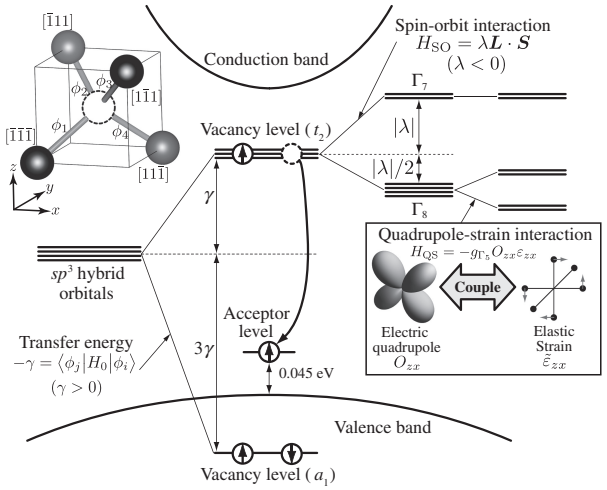

Fig. 1. Level scheme of the vacancy orbital in boron-doped silicon. The sp^3 dangling bond of ϕ_i for $i = 1$, 2, 3, and 4 splits into an a_1 singlet state and a t_2 triplet state due to the transfer energy of $\langle \phi_i | H_0 | \phi_j \rangle = -\gamma$ $(i \neq j)$. The dopant-boron state accepts an electron from the triplet state of the vacancy orbital. The spin–orbit interaction $H_{SO} = \lambda \boldsymbol{L} \cdot \boldsymbol{S}$ $(\lambda < 0)$ with spin $S = 1/2$ and orbital $L = 1$ gives rise to the Γ_8 quartet ground state and Γ_7 doublet excited state. The elastic strain ε_{zx} of the ultrasonic wave couples to the electric quadrupole O_{zx} of the vacancy orbital.

quadrupole-strain interaction constant still remains to be performed.[6–8)]

In the present paper, we demonstrate the low-temperature ultrasonic measurements and infrared laser tomography measurements on a boron-doped silicon ingot grown by the Czochralski (CZ) method. The procedures of the crystal growth using the CZ method and the low-temperature ultrasonic measurements are presented in Sect. 2. We show the defect characterization of the CZ ingot in Sect. 3.1, the variation in the elastic softening depending on the position of the ingot in Sect. 3.2, the distribution of voids observed by laser scattering tomography in Sect. 3.3, and a sum rule between residual vacancies and consumed vacancies in the formation of voids in Sect. 3.4. We discuss the quadrupole susceptibility of the vacancy orbital and determination of the quadrupole-strain interaction constant in Sect. 4. We present our conclusions in Sect. 5.

2. Experiment

A single-crystalline boron-doped CZ silicon ingot for wafers with a diameter of 300 mm was grown in the facility of GlobalWafers Japan in Niigata. The pulling rate during the crystal growth and the temperature gradient at the solid-melt interface in the CZ furnace were carefully controlled to prepare high-quality silicon wafers. The resistivity 24–25 Ω·cm of the ingot indicates a boron-dopant concentration about 5×10^{14} atoms cm^{-3}. Cu-decorated X-ray topography was employed to distinguish between voids and dislocation loops in the grown-in defect regions. X-ray topography can be used to distinguish between a vacancy rich N_v and an interstitial rich N_i in the neutral region.

We have carried out infrared laser scattering tomography to observe voids in the wafers. The scattering intensity of the laser beam with a wavelength $\lambda = 1064$ nm can be used to detect voids with sizes from 19 to 150 nm.[14,15)] The distribution of the voids in the wafers was observed by laser beam scanning over the wafers. From the intensity of the light scattered by individual voids, we evaluated the size of the voids. Taking the size and density of the voids in the silicon wafer into account, we deduce the amount of the vacancies consumed in the formation of the voids.

The samples for the present ultrasonic measurements were cut out from wafers with a 0.775 mm thickness and from specially prepared blocks with a 3.0 mm thickness. Both sides of the wafers and blocks were polished by a standard manufacturing process. We used an ultrasonic pulse echo method to measure the ultrasonic velocity in the boron-doped silicon. The wafers and blocks used in the present experiments were annealed in ambient N_2 at 650 °C for 30 min, in which the thermal donors were annihilated to properly prepare p-type carriers. The transverse ultrasonic wave for the elastic constant C_{44} was particularly adopted for the evaluation of the vacancy concentration by measuring low-temperature softening, because the softening of C_{44} is more pronounced than that of $(C_{11} - C_{12})/2$.[6)] The piezoelectric $LiNbO_3$ transducer of the X-cut with a 40 μm thickness with a fundamental resonance frequency of 45 MHz was employed for the generation and detection of transverse ultrasonic waves. The transverse ultrasonic wave propagating along the [001] axis with the polarization vector along the [100] axis induces the elastic strain ε_{zx} in the lattice. The elastic constant $C_{44} = \rho v^2$ is obtained using a density $\rho = 2.33$ g cm^{-3} and the sound velocity v measured using transverse ultrasonic waves.

The low-temperature softening of C_{44} down to 30 mK was measured using a dilution refrigerator (Kelvinox 400HA, Oxford Instruments). The eight coaxial lines were installed for the simultaneous measurements of four silicon samples. An oxygen-free copper rod with a 10 mm diameter was used for thermal contact from a mixing chamber to a sample holder consisting of a silver plate. The temperature of the silicon samples was measured using the calibrated RuO_2 resistance thermometer RX-102B (Lake Shore Cryotronics).

3. Results

3.1 Cross-sectional view of the CZ ingot

In Fig. 2(a), we show a cross-sectional view of the boron-doped CZ ingot investigated in the present experiments. The vertical axis of Fig. 2(a) denotes the relative pulling rate V in arbitrary units in the crystal growth. The ratio V/G of the pulling rate V to the temperature gradient G over the solid-melt interface determines the character of the grown-in defects in the CZ ingot.[16)] A high pulling rate favors the void-rich region, while a relatively low pulling rate leads to the anomalous oxygen precipitation (AOP) region.[17)] The oxidation stacking fault (OSF) region located between void and AOP regions was supposed from the results of the Cu-decorated X-ray topography. With further reduction in the pulling rate, the vacancy-rich neutral region N_v crosses over to the interstitial-rich neutral region N_i.

The fast crystal cooling process when rapidly leaving from the solid-melt interface in the CZ furnace creates vacancies of high concentration, which lead to void formation. In other words, vacancies dissolved in the host silicon lattice at excess concentration gather into a "negative crystal". Each void is octahedral, and 100 nm in typical size.[2)] In semiconductor device production, voids in a silicon wafer lead to serious

©2013 The Physical Society of Japan

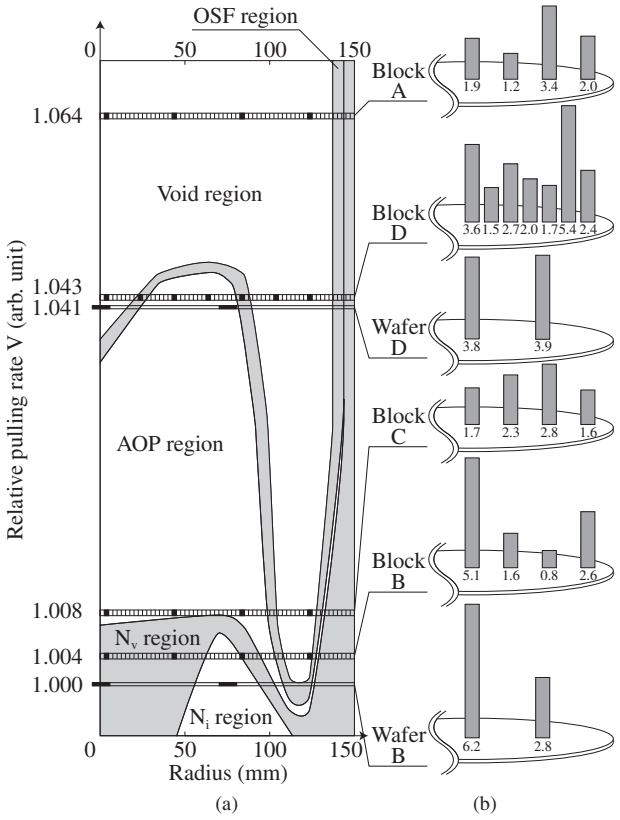

Fig. 2. (a) Cross-sectional view of the grown-in defect regions consisting of void, OSF, AOP, N_v, and N_i regions in a boron-doped CZ silicon ingot with a diameter of 300 mm. The vertical axis represents the relative pulling rate V in arbitrary units. Blocks A, D, C, and B were specially prepared with a 3.0 mm thickness. Wafers D and B were prepared with a standard thickness of 0.775 mm. The closed squares in (a) indicate the samples used in the ultrasonic measurements. The bar graphs in (b) indicate the amount of softening of $\Delta C_{44}/C_{44}$ at various positions in the blocks and wafers. The numerical values of the softening of $\Delta C_{44}/C_{44}$ in 10^{-5} units in (b) are given at the bottom of the bar graphs.

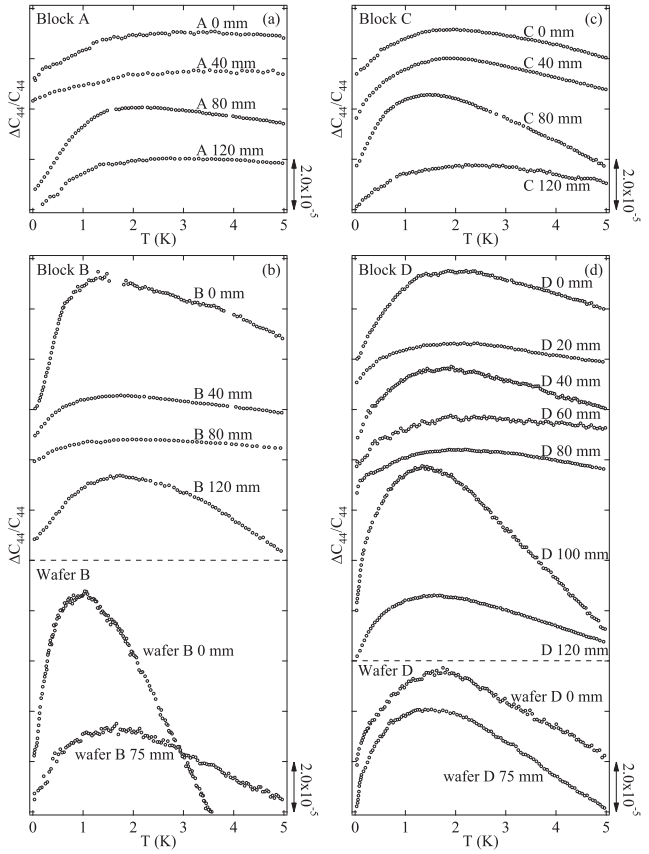

Fig. 3. Low-temperature softening of $\Delta C_{44}/C_{44}$ below about 2 K down to 30 mK of the silicon samples taken from block A in (a), block B and wafer B in (b), block C in (c), and block D and wafer D in (d). We adopt the label A ℓ mm, for instance, to indicate the position of the sample at a distance of ℓ mm from the center of the block or wafer.

unwanted effects on the electronic properties of the device. Epitaxial and annealed wafers are currently adopted to overcome serious reduction in yield due to voids.

In the present work, we evaluate residual and consumed vacancies for void formation in the samples, which were cut from the characteristic grown-in defect regions of the ingot in Fig. 2(a). Specially prepared blocks of A, D, C, and B with a 3 mm thickness and wafers D and B with a standard thickness of 0.775 mm were used. Block A was taken from the void region. Wafer D and block D were located in the crossover area from the void region to the AOP region across the OSF region. Wafer D was beneath block D. Block C includes the AOP, OSF, void, and N_v regions. Block B and wafer B were taken from the region consisting of the N_v, N_i, AOP, OSF, and void regions. The closed squares in Fig. 2(a) indicate the positions of the samples measured in the present ultrasonic experiments.

3.2 *Elastic softening in C_{44} depending on positions in the ingot*

In order to determine the concentration of the vacancies in the blocks and wafers, we measured the low-temperature elastic softening of C_{44} below about 2 K down to 30 mK of block A in Fig. 3(a), block B and wafer B in Fig. 3(b), block C in Fig. 3(c), and block D and wafer D in Fig. 3(d). The label A 120 mm in Fig. 3(a), for instance, denotes a distance of 120 mm from the center of block A. The most pronounced softening of $\Delta C_{44}/C_{44} = 6.5 \times 10^{-5}$ was observed for wafer B 0 mm at the center of the wafer B in Fig. 3(b). The amount of softening of $\Delta C_{44}/C_{44}$ is shown by the height of bar graphs in Fig. 2(b) for transparent insight. The numerical values of the softening of $\Delta C_{44}/C_{44}$ in 10^{-5} units below about 2 K down to 30 mK are also presented at the bottom of the bar graphs of Fig. 2(b). As is shown in Eq. (5) in Sect. 4, the amount of elastic softening of C_{44} is proportional to the vacancy concentration N in the silicon crystal. Consequently, the appreciable distribution of the softening in the bar graph in Fig. 2(b) evidences the vacancy distribution depending on the positions in the blocks and wafers taken from the ingot.

The N_v and N_i regions in Fig. 2(a) can be distinguished from each other using X-ray topography for the silicon wafer, in which thermal annealing for 3 h at 780 °C and then for 16 h at 1000 °C was carried out. The resultant oxygen precipitation was imaged as X-ray haze in the topography. It is assumed that vacancies accelerate oxygen precipitation, while silicon interstitials are irrelevant for such precipitation. X-ray topography can therefore be used to distinguish the N_v region from the N_i region.

The softening of $\Delta C_{44}/C_{44} = 2.8 \times 10^{-5}$ of wafer B 75 mm in the N_i region is larger than that of $\Delta C_{44}/C_{44} =$

©2013 The Physical Society of Japan

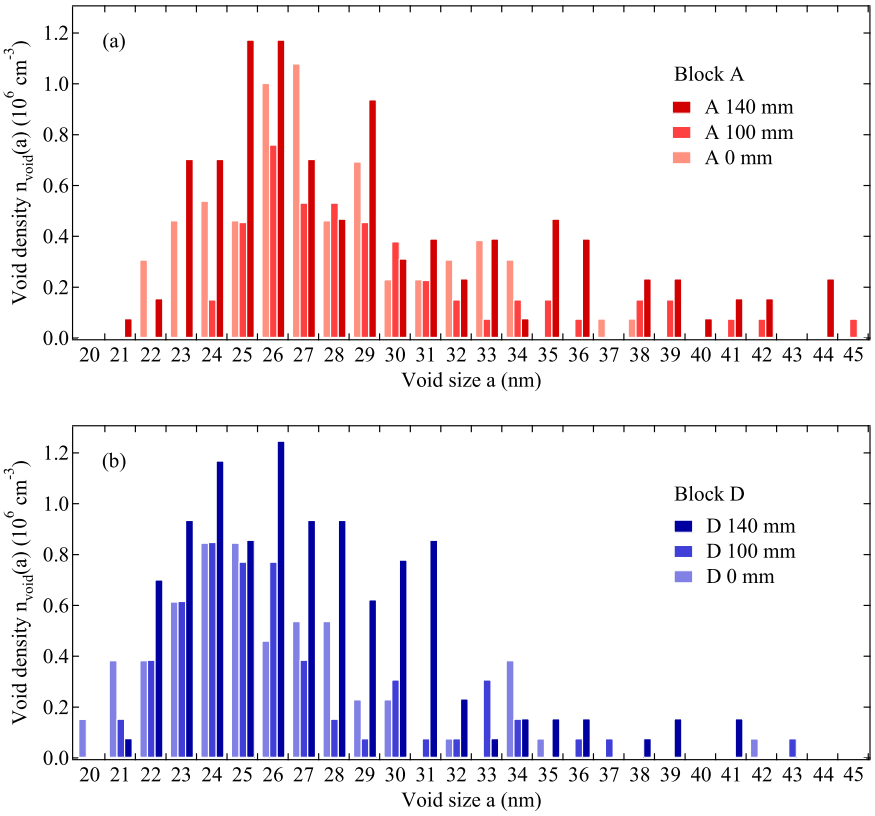

Fig. 4. (Color online) Void density $n_{void}(a)$ for void sizes a from 20 up to 45 nm in the silicon samples of block A in (a) and block D in (b). Colors of the bar graphs correspond to the radial positions in the blocks. Laser scattering tomography was used for estimating the size and density of the voids.

1.6×10^{-5} of B 40 mm and that of $\Delta C_{44}/C_{44} = 0.8 \times 10^{-5}$ of B 80 mm in the N_v region. The contradiction in results suggests that the oxygen precipitation is affected not only by the vacancy concentration but also by other unknown factors. Consequently, low-temperature softening by the ultrasonic measurement can be used to directly observe the vacancy concentration, while X-ray topography can be used to detect the oxygen precipitation. Thus, the low-temperature ultrasonic method is invaluable for vacancy evaluation in wafers.

3.3 *Voids observed by laser scattering tomography*

We have carried out laser scattering tomography to evaluate the void density $n_{void}(a)$ as a function of the void size a in the wafers, which were taken from the wafer adjacent to the wafers or blocks in the ingot used in the ultrasonic measurements. The observed distribution $n_{void}(a)$ at the radial positions of 0, 100, and 140 mm from the center of block A is shown as bar graphs in Fig. 4(a). Figure 4(b) shows the void distributions at 0, 100, and 140 mm from the center of block D. The void size a in the bar graphs of $n_{void}(a)$ in block A in Fig. 4(a) and those in block D in Fig. 4(b) range from 20 to 45 nm. The distribution of the void density $n_{void}(a)$ in Figs. 4(a) and 4(b) commonly exhibits a maximum $n_{void}(a) = 1.2 \times 10^6\,\mathrm{cm}^{-3}$ around the void size a in the range of 25–26 nm.

We estimate the amount of vacancies consumed in void formation. The volume of a vacancy is regarded as the volume of a silicon atom, $V_{Si} = 2 \times 10^{-23}\,\mathrm{cm}^3$, in the lattice. An octahedral void of size a has a volume $V_{void}(a) = \sqrt{2}a^3/3$. Summing up the observed voids densities $n_{void}(a)$ with respect to a in the range of 19–45 nm of block A in Fig. 4(a) and of block D in Fig. 4(b), we estimate the total amount of consumed vacancies in void formation as

$$N_{cons} = \frac{\sum_a n_{void}(a) V_{void}(a)}{V_{Si}} = \frac{\sum_a n_{void}(a) \frac{\sqrt{2}}{3} a^3}{V_{Si}}. \quad (1)$$

The N_{cons} at various radial positions in blocks A, B, C, and D are shown together in Fig. 5. The consumed vacancies of block A cut out from the void region and of block D slightly reaching the OSF and AOP regions exhibit two maxima with $N_{cons} = 4.5 \times 10^{12}\,\mathrm{cm}^{-3}$ at the radial position of 20 mm from the center and $N_{cons} = 8.5 \times 10^{12}\,\mathrm{cm}^{-3}$ at the radial position of 120 mm. On the other hand, block C cut out from the neutral region and block B from the N_v–N_i–N_v–AOP region have one common peak with $N_{cons} = 3.0 \times 10^{12}\,\mathrm{cm}^{-3}$ at a radial position of 130 mm from the center.

It has been reported that tomography with laser scattering can be used to detect voids larger than 20 nm.[18] The rapid decrease in the void density $n_{void}(a)$ with the reduction in void size to the lower limit of 20 nm in Figs. 4(a) and 4(b) is not due to the experimental conditions for tomography. It may be caused by the intrinsic feature that the distribution of the void density $n_{void}(a)$ mostly follows a normal distribution with an expected value of about 26 nm.[18] Since the distribution of the voids below 20 nm is out of the scope of laser scattering tomography, the consumed vacancies in Eq. (1) is regarded as the lower limit in the experimental

©2013 The Physical Society of Japan

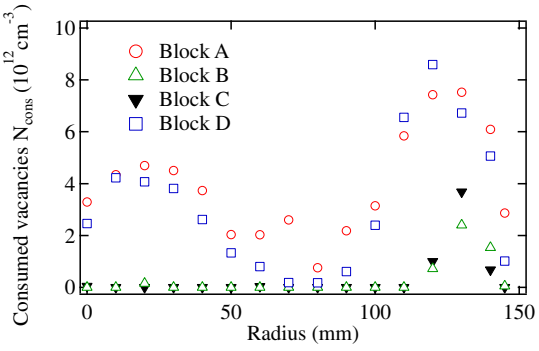

Fig. 5. (Color online) Amounts of consumed vacancies N_{cons} in void formation for the samples taken from blocks A, B, C, and D. The density $n_{void}(a)$ and size a of the voids obtained by laser scattering tomography were used to estimate N_{cons}.

estimation by the tomography. Nevertheless, it worthwhile to calculate the quadrupole-strain interaction constant in Sect. 4 using the consumed vacancies obtained by laser tomography.

3.4 *Correlation of softening in C_{44} and consumed vacancies for void formation*

In Fig. 6, we show the amount of softening of $\Delta C_{44}/C_{44}$ versus the consumed vacancies N_{cons} in blocks A and D. The open circles denote the results for block A located in the void region. The open triangles denote the results for block D located across the void–OSF–AOP region. As regards the inner regions of blocks A and D in Fig. 2(a), the ratio V/G of the pulling rate V to the temperature gradient G is expected to be constant. The total number of vacancies N_{cons} created initially is also expected to be constant. Actually, the solid and dashed lines in Fig. 6 evidence the sum rule of $N_{total} = N + N_{cons}$ for the residual vacancies N and the consumed vacancies N_{cons}. The intersection of the solid line across the vertical axis means the total amount of vacancies $N_{total} = 5.9 \times 10^{12}\,\mathrm{cm}^{-3}$, which corresponds to the vacancies initially created in the inner areas 0, 40, and 80 mm from the center of block A during the ingot growth. The dashed line for the samples of 0, 20, and 40 mm in block D intersects the vertical axis at $N_{total} = 7.4 \times 10^{12}\,\mathrm{cm}^{-3}$, which also corresponds to the vacancies initially created in the void, OSF, and AOP regions during the ingot growth.

The number of vacancies $N_{cons} = 3.1 \times 10^{12}\,\mathrm{cm}^{-3}$ consumed in void formation for the A 0 mm sample in Fig. 6 was obtained from the laser scattering tomography results in Fig. 5. When we adopt the sum rule of $N_{total} = N + N_{cons}$, we successfully deduce the residual vacancies $N = 2.8 \times 10^{12}\,\mathrm{cm}^{-3}$ for A 0 mm sample. A similar procedure has been done for estimation of the residual vacancies N in D 0 mm sample in Fig. 6. The consumed vacancies $N_{cons} = 2.1 \times 10^{12}\,\mathrm{cm}^{-3}$ was obtained by laser scattering tomography in Fig. 5. Adopting the sum rule of $N_{total} = N + N_{cons}$ for block D, we deduce $N = 5.3 \times 10^{12}\,\mathrm{cm}^{-3}$ for the D 0 mm sample. Taking the one-to-one correspondence of the residual vacancy concentration to the amount of low-temperature softening into account, we deduce that low-temperature softening in $\Delta C_{44}/C_{44} = 1.0 \times 10^{-4}$ units directly gives the absolute value of the vacancy concentration $N = 1.5 \times 10^{13}\,\mathrm{cm}^{-3}$ in boron-doped CZ silicon.

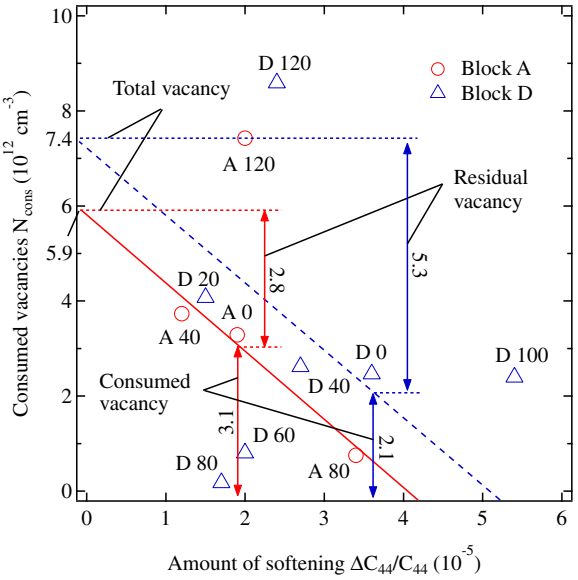

Fig. 6. (Color online) Correlation between the consumed vacancies N_{cons} and the softening of $\Delta C_{44}/C_{44}$ in void formation in blocks A and D. This correlation evidences the sum rule of N_{cons} in void formation and the residual vacancies N estimated by low-temperature softening.

Under the equilibrium condition, the ratio of the formation energy of vacancy to the melting temperature governs vacancy creation in crystals. However, the CZ furnace for growing a silicon ingot with a 300 mm diameter is actually regarded as a nonequilibrium system, where the pulling rate V and the temperature gradient G over the solid-melt surface determine N_{total}, i.e., the amount of created vacancies.[16,19] The supersaturation of vacancies brings about voids, namely, "negative crystals" with an octahedral shape. The conditions for void formation were investigated using a simulation model,[18] but the numerical analysis of the correlation between residual vacancy and consumed vacancy is beyond the scope of this study.

As one can see in Fig. 6, the amount of consumed vacancies in voids formation of the A 120 mm sample in block A is higher than that of A 0, A 40, and A 80 mm samples. The consumed vacancies of the D 120 mm sample in block D is also larger than those of the D 0, D 20, and D 40 mm samples. This result is naturally accounted for by the fact that the total sum of vacancies created in the outer region of the ingot is larger than that in the inner region of the ingot, because the ratio V/G effectively increases in the outer region.

4. Discussion

Transverse ultrasonic waves propagating along the [001] axis with a polarization vector parallel to the [100] axis induce the elastic strain ε_{zx} in the silicon lattice. The low-temperature softening of C_{44} in Fig. 3 is caused by the interaction of the elastic strain ε_{zx} with the Γ_5 symmetry with the electric quadrupole O_{zx} with the same symmetry of a vacancy orbital.[6–8,20] The perturbation Hamiltonian for the quadrupole-strain interaction in unit volume is written as[21,22]

©2013 The Physical Society of Japan

$$H_{\mathrm{QS}} = -g_{\Gamma_5} \sum_i O^i_{zx} \varepsilon_{zx}. \tag{2}$$

Here, g_{Γ_5} is the interaction constant and O^i_{zx} denotes the electric quadrupole of the vacancy orbital at the i-th site. $\sum_i$ denotes summing over the vacancy site i in unit volume. Taking the operator equivalent into account, we write the electric quadrupole as $O_{zx} = L_z L_x + L_x L_z$. Here, L_x and L_z are the components of the angular momentum of the vacancy orbital. The total free energy consisting of the elastic energy due to the ultrasonic wave and the vacancy orbital is written as

$$F = \frac{1}{2} C^0_{44} \varepsilon^2_{zx} - k_{\mathrm{B}} T \ln \left[\sum_j \exp\left(-\frac{E_j(\varepsilon_{zx})}{k_{\mathrm{B}} T} \right) \right]^N. \tag{3}$$

Here, C^0_{44} is the elastic constant when the quadrupole-strain interaction is absent. N is the number of vacancies in unit volume. The perturbation energy of $E_j(\varepsilon_{zx})$ for the Γ_8–Γ_7 states of the vacancy orbital at the cubic T_d site symmetry is calculated using the perturbation Hamiltonian of Eq. (2) as a function of the strain ε_{zx} in processes up to the second order. The elastic softening is also affected by the quadrupole intersite interaction as

$$H_{\mathrm{QQ}} = -\sum_{i>j} K_{ij} O^i_{zx} O^j_{zx} = -g'_{\Gamma_5} \sum_i \langle O_{zx} \rangle O^i_{zx}. \tag{4}$$

Here, K_{ij} is the interaction constant between the vacancy orbitals at the i-th and j-th sites. g'_{Γ_5} is the interaction constant for a mean field value $\langle O_{zx} \rangle$ of the quadrupole. Taking the Hamiltonians of Eqs. (2) and (4) into account, the temperature dependence of the elastic constant C_{44} is obtained as

$$C_{44} = C^0_{44} - \frac{N g^2_{\Gamma_5} \chi_{\Gamma_5}}{1 - g'_{\Gamma_5} \chi_{\Gamma_5}}, \tag{5}$$

where χ_{Γ_5} denotes the quadrupole susceptibility for the vacancy orbital as

$$-g^2_{\Gamma_5} \chi_{\Gamma_5}(T) = \left\langle \frac{\partial^2 E_j(\varepsilon_{zx})}{\partial \varepsilon^2_{zx}} \right\rangle - \frac{1}{k_{\mathrm{B}} T} \left\{ \left\langle \left(\frac{\partial E_j(\varepsilon_{zx})}{\partial \varepsilon_{zx}} \right)^2 \right\rangle - \left\langle \frac{\partial E_j(\varepsilon_{zx})}{\partial \varepsilon_{zx}} \right\rangle^2 \right\}. \tag{6}$$

Here, $\langle A \rangle$ means the thermal average of the quantity A. The first term on the right-hand side in Eq. (6) denotes the van Vleck term due to off-diagonal processes. The second term denotes the Curie term due to diagonal processes. The Curie term exhibits a pronounced temperature dependence proportional to the reciprocal temperature, while the van Vleck term shows a temperature-independent behavior at low temperatures.

The steep low-temperature softening of C_{44} of boron-doped silicon is caused by the Curie term due to the Γ_8 ground state with orbital degeneracy. In the present analysis, we adopt the eigen functions of the Γ_8 ground and Γ_7 excited states as[8]

$$|\Gamma_7\rangle \begin{cases} |\alpha\rangle = \sqrt{\frac{2}{3}} \left| 1, -\frac{1}{2} \right\rangle - \frac{1}{\sqrt{3}} \left| 0, \frac{1}{2} \right\rangle \\ |\beta\rangle = \sqrt{\frac{2}{3}} \left| -1, \frac{1}{2} \right\rangle - \frac{1}{\sqrt{3}} \left| 0, -\frac{1}{2} \right\rangle \end{cases},$$

$$|\Gamma_8\rangle \begin{cases} |\nu\rangle = \frac{1}{\sqrt{3}} \left| 1, -\frac{1}{2} \right\rangle + \sqrt{\frac{2}{3}} \left| 0, \frac{1}{2} \right\rangle \\ |\kappa\rangle = \frac{1}{\sqrt{3}} \left| -1, \frac{1}{2} \right\rangle + \sqrt{\frac{2}{3}} \left| 0, -\frac{1}{2} \right\rangle \\ |\lambda\rangle = \left| 1, \frac{1}{2} \right\rangle \\ |\mu\rangle = \left| -1, -\frac{1}{2} \right\rangle \end{cases}. \tag{7}$$

Here, $|M_L, M_S\rangle$ in Eq. (7) denotes the wave function for the magnetic quantum number $M_L = 1, 0, -1$ for the angular momentum $L = 1$ and $M_S = 1/2, -1/2$ for spin $S = 1/2$.

The Γ_8 quartet state with a special unitary group SU(4) symmetry has three magnetic dipoles, five electric quadrupoles, and seven magnetic octupoles.[23,24] Among these multipoles, the electric quadrupoles couple to the appropriate elastic strains. We refer to the low-temperature softening of the elastic constants of the rare-earth compounds CeB_6 and $Ce_3Pd_{20}Ge_6$ with the Γ_8 quartet ground state.[25,26] The quadrupole susceptibility of Eq. (6) for the vacancy orbital with the Γ_8 ground and Γ_7 excited states of Eq. (7) is written as

$$\chi_{\Gamma_5}(T) = \frac{2}{3} \left(2 + \exp\left[\frac{3}{2} \lambda \frac{1}{k_{\mathrm{B}} T} \right] \right)^{-1} \times \left\{ \frac{1}{k_{\mathrm{B}} T} - \frac{4}{3\lambda} \left(1 - \exp\left[\frac{3}{2} \lambda \frac{1}{k_{\mathrm{B}} T} \right] \right) \right\}. \tag{8}$$

Here, we adopted the energy gap $\Delta = -3\lambda/2 = 1\,\mathrm{K}$ for the Γ_8 ground state and Γ_7 excited states due to the spin–orbit interaction to properly explain the softening.

As shown in Eqs. (5) and (6), the softening of C_{44} is proportional to $N g^2_{\Gamma_5}$, namely, the product of the residual vacancies N and the square of the interaction constant $g^2_{\Gamma_5}$ of the quadrupole-strain interaction. The low-temperature softening of C_{44} of the A 0 mm sample taken from the center in block A of Fig. 7(a) and in the D 0 mm sample from the center in the block D of Fig. 7(b) are well fitted by Eqs. (5) and (6). The solid lines give $N g^2_{\Gamma_5} = 2.4 \times 10^{23}\,\mathrm{K^2/cm^3}$ and $g'_{\Gamma_5} = -1.0\,\mathrm{K}$ for the A 0 mm sample in Fig. 7(a) and $N g^2_{\Gamma_5} = 4.0 \times 10^{23}\,\mathrm{K^2/cm^3}$ and $g'_{\Gamma_5} = -0.9\,\mathrm{K}$ for the sample D 0 mm in Fig. 7(b). Here, the dashed lines in Figs. 7(a) and 7(b) indicate the background C^0_{44} of the elastic constant when the quadrupole-strain interaction is omitted. The temperature dependence C^0_{44} due to the anharmonic properties of the lattice is written as[22]

$$C^0_{44} = C^0 - \frac{s}{\exp(t/T) - 1}. \tag{9}$$

In fitting of Fig. 7, we adopt $C^0 = 8.06266$ (8.06308) in $10^{10}\,\mathrm{J/m^3}$ units, $s = 1.35 \times 10^6\,\mathrm{J/m^3}$ ($2.85 \times 10^6\,\mathrm{J/m^3}$) and $t = 6.0\,\mathrm{K}$ (4.1 K) for the softening of the A 0 mm sample in (a) [of the D 0 mm sample in (b)].

In Fig. 8, we picture a solid line of $N g^2_{\Gamma_5} = 2.4 \times 10^{23}\,\mathrm{K^2/cm^3}$ for the A 0 mm sample as a function of the residual vacancy concentration N versus the quadrupole-strain interaction constant g_{Γ_5}. Adopting the residual vacancy concentration $N = 2.8 \times 10^{12}\,\mathrm{cm^{-3}}$ for the A 0 mm sample, we obtain the quadrupole-strain interaction constant $g_{\Gamma_5} = (2.93 \pm 0.2) \times 10^5\,\mathrm{K}$ per vacancy in the boron-doped silicon. Furthermore, the dashed line of

©2013 The Physical Society of Japan

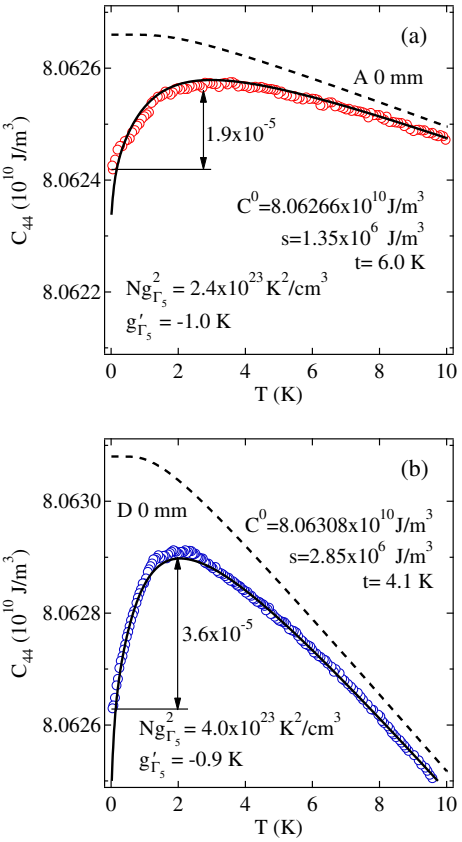

Fig. 7. (Color online) Theoretical fitting of the low-temperature softening due to the vacancy orbital for the boron-doped silicon A 0 mm sample in (a) and D 0 mm sample in (b). The solid lines are fits in terms of $C_{44} = C^0_{44} - Ng^2_{\Gamma_5}\chi_{\Gamma_5}/(1 - g'_{\Gamma_5}\chi_{\Gamma_5})$ of Eq. (5). The quadrupole susceptibility χ_{Γ_5} of Eq. (8) is responsible for the Γ_8 ground and Γ_7 excited states at 1 K of the vacancy orbital. The dashed lines are backgrounds showing the temperature dependence of Eq. (9) in the text.

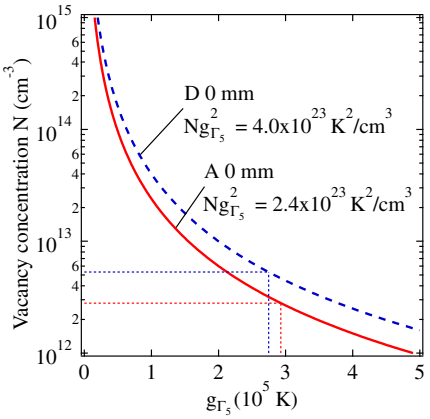

Fig. 8. (Color online) Relationship of the residual vacancy concentration N and the quadrupole-strain interaction constant g_{Γ_5} for the A 0 mm and D 0 mm samples. Here, we adopt $Ng^2_{\Gamma_5} = 2.4 \times 10^{23}$ K/cm^3 and $N = 2.8 \times 10^{12}$ cm^{-3} for the A 0 mm sample in Fig. 7(a) and $Ng^2_{\Gamma_5} = 4.0 \times 10^{23}$ K/cm^3 and $N = 5.3 \times 10^{12}$ cm^{-3} for the D 0 mm sample in Fig. 7(b). We successfully deduce the quadrupole-strain interaction constant $g_{\Gamma_5} = (2.8 \pm 0.2) \times 10^5$ K per vacancy orbital with the Γ_8–Γ_7 states in boron-doped silicon.

$Ng^2_{\Gamma_5} = 4.0 \times 10^{23}$ K^2/cm^3 for the D 0 mm sample in Fig. 8 leads to the interaction constant $g_{\Gamma_5} = (2.75 \pm 0.2) \times 10^5$ K per vacancy using the residential vacancies $N = 5.3 \times 10^{12}$ cm^{-3}.

Taking the experimental errors into account, we deduced the strong interaction constant of $g_{\Gamma_5} = (2.8 \pm 0.2) \times 10^5$ K per vacancy for the quadrupole-strain interaction, which is one of the most striking features of the vacancy orbital with an extended radius of up to 1 nm. The deformation energy d is defined as the eigenvalue of the quadrupole strain interaction, $H_{\rm QS} = g_{\Gamma_5} O_{zx}\varepsilon_{zx}$, for the unit strain ε_{zx}. We fixed the huge deformation energy d at 1.6×10^5 K because $g_{\Gamma_5}\langle\Gamma_8|O_{zx}|\Gamma_8\rangle \sim 2.8 \times 10^5/\sqrt{3} = 1.6 \times 10^5$ K of the vacancy orbital, where the absolute value of eigenvalue of $\langle\Gamma_8|O_{zx}|\Gamma_8\rangle$ is $1/\sqrt{3}$. Even a tiny strain of $\varepsilon_{zx} = 10^{-5}$ in the silicon brings about an observable change of 1.6 K in the energy of the vacancy orbital. As was pointed out in Sect. 3.3, the consumed vacancies estimated by laser tomography corresponds to the lower limit. Therefore, the interaction constant $g_{\Gamma_5} = (2.8 \pm 0.2) \times 10^5$ K determined is regarded as the higher limit. The improvement of laser scattering tomography for observing voids with sizes less than 20 nm would be required.

The extended radius of a vacancy orbital up to 1 nm leads to the slow electron.[13] Actually, the energy gap 1 K of the Γ_8–Γ_7 states of the vacancy orbital due to the spin–orbit interaction, which is caused by the relativistic motions of electrons, is considerably small as compared with those of $\sim 5 \times 10^2$ K for transition-metal compounds and $\sim 5 \times 10^3$ K for rare-earth compounds.[27,28] The low electron velocity and strong quadrupole-strain interaction of the vacancy orbital require a rigorous theoretical approach to the electron–lattice interaction system beyond the adiabatic approximation.

The present experimental results clearly indicate that the vacancy site of the boron-doped silicon currently used in the semiconductor industry possesses a cubic T_d site symmetry even at the base temperature of 20 mK. This is definitely different from the symmetry breaking features observed in sufficiently irradiated silicon samples with vacancies at high concentrations of 10^{16}–10^{18} cm^{-3}.[29,30] A high concentration of vacancies in the artificially irradiated silicon samples may induce local distortions due to intersite quadrupole interactions through strain fields. This resembles the emergence of spin glass phases due to the intersite magnetic interaction in magnetic impurity systems.

The present silicon ingot currently used in semiconductor industry has a very low vacancy concentration range of 10^{12}–10^{13} cm^{-3}. Here, note that the wafer has a silicon density $N_{\rm Si} = 5 \times 10^{22}$ cm^{-3}. The vacancies in the wafer distribute at a mean distance of $\sim 1 \times 10^3$ between silicon atoms. The vacancy concentration in the present wafer is too low to induce the cooperative Jahn–Teller distortion. The ground state of a vacancy orbital at low temperatures in boron-doped silicon may be understood in terms of the vibronic state of the vacancy orbital, which is strongly coupled to the surrounding lattice vibration.[31,32] This situation resembles the Kondo singlet formation in magnetic metals, where localized electrons with a spin bind to conduction electrons due to the antiferromagnetic exchange interaction without symmetry-breaking transition.[33,34]

5. Concluding Remarks

We have carried out ultrasonic measurements of silicon wafers prepared from a boron-doped CZ ingot with a

©2013 The Physical Society of Japan

diameter of 300 mm in order to determine the quadrupole-strain interaction constant of a vacancy orbital. The characteristic distribution of low-temperature softening of C_{44} below 2 K down to 30 mK shows the distribution of the vacancy concentration in the ingot. We also carried out laser scattering tomography to measure the size and density of voids and evaluated the consumed vacancies in void formation. At the center of the wafers taken from the void region of the ingot, we found a correlation between low-temperature softening and the consumed vacancies in void formation. The correlation evidences the sum rule of the residual and consumed vacancies for void formation. Taking the sum rule of the residual and consumed vacancies in the ingot into account, we deduced the numerical value of the interaction constant $g_{\Gamma_5} = (2.8 \pm 0.2) \times 10^5$ K in the quadrupole-strain interaction for a vacancy orbital in boron-doped silicon. The large interaction constant is due to the enhancement of the electric quadrupole of the vacancy orbital with an extended radius of up to 1 nm. The one-to-one correspondence between the softening of $\Delta C_{44}/C_{44} = 1.0 \times 10^{-4}$ below 2 K down to 30 mK and the vacancy concentration $N = 1.5 \times 10^{13}$ cm^{-3} allowed us to determine the vacancy concentration by low-temperature ultrasonic measurements. The experimental determination of the quadrupole-strain interaction constant in this work will open a gate to an innovative technology for vacancy evaluation in silicon wafers currently used in semiconductor industry.

There is a continuing trend toward higher device densities for complementary metal oxide semiconductors in pursuit of large-capacity memory devices and high-speed processors. Frontline researchers on LSI devices pursue the process rule beyond 19 nm. It is desirable for semiconductor industry to adopt low-temperature ultrasonic measurements for the evaluation of the absolute value of vacancies in silicon wafers as one of the figure of merits, because it is indeed valuable to realize innovative 450 mm silicon wafers in the future.

Acknowledgments

We thank Akira Hasegawa and Takehiko Bando of Niigata University for continuous support of the present work attempting to apply of solid state physics to semiconductor technology. We also thank Masashi Muromachi and Syouzou Saito of Toshiba Corporation and Susumu Kouyama of GlobalWafers Japan Co., Ltd. for support of the present basic research pursuing an innovative semiconductor technology for vacancy evaluation. We appreciate the financial support by "The Innovation Research Project on Nano-electronics Materials and Structure" from the Ministry of Economy, Trade and Industry of Japan. This work was partly supported by a Grant-in-Aid for Specially Promoted Research (No. 18002008) "Strongly correlated quantum phases associated with charge fluctuations" from the Ministry of Education, Culture, Sports, Science and Technology of Japan. We acknowledge the support through the Strategic Young Researcher Overseas Visits Program for Accelerating Brain Circulation from the Japan Society for the Promotion of Science (JSPS). We also acknowledge the support in the form of a Grant-in-Aid for Scientific Research "Supporting Program for Creating University Ventures" from the Japan Science and Technology Agency. This work was also supported by the Strategic Project of Education and Research of Niigata University.

*goto@phys.sc.niigata-u.ac.jp

1) The International Technology Roadmap for Semiconductors (ITRS), 2011 edition [http://www.itrs.net].
2) M. Kato, T. Yoshida, Y. Ikeda, and Y. Kitagawara: Jpn. J. Appl. Phys. **35** (1996) 5597.
3) J. Ryuta, E. Morita, T. Tanaka, and Y. Shimanuki: Jpn. J. Appl. Phys. **29** (1990) L1947.
4) H. Harada, T. Abe, and J. Chikawa: in *Semiconductor Silicon 1986*, ed. H. R. Huff, T. Abe, and B. O. Kolbesen (Electrochemical Society, Pennington, NJ, 1986) p. 76.
5) M. Hourai, T. Nagashima, E. Kajita, S. Sumita, M. Sano, and T. Shigematsu: in *Semiconductor Silicon 1994*, ed. H. R. Huff, W. Bergholz, and K. Sumino (Electrochemical Society, Pennington, NJ, 1994) p. 156.
6) T. Goto, H. Yamada-Kaneta, Y. Saito, Y. Nemoto, K. Sato, K. Kakimoto, and S. Nakamura: J. Phys. Soc. Jpn. **75** (2006) 044602.
7) S. Baba, T. Goto, Y. Nagai, M. Akatsu, H. Watanabe, K. Mitsumoto, T. Ogawa, Y. Nemoto, and H. Yamada-Kaneta: J. Phys. Soc. Jpn. **80** (2011) 094601.
8) S. Baba, M. Akatsu, K. Mitsumoto, S. Komatsu, K. Horie, Y. Nemoto, H. Yamada-Kaneta, and T. Goto: J. Phys. Soc. Jpn. **82** (2013) 084604.
9) C. A. Coulson and M. J. Kearsley: Proc. R. Soc. London, Ser. A **241** (1957) 433.
10) H. Matsuura and K. Miyake: J. Phys. Soc. Jpn. **77** (2008) 043601.
11) T. Ogawa, K. Tsuruta, H. Iyetomi, H. Y. Kaneta, and T. Goto: MRS Proc. **1195** (2009) B08.
12) T. Yamada, Y. Yamakawa, and Y. Ōno: J. Phys. Soc. Jpn. **78** (2009) 054702.
13) T. Ogawa, K. Tsuruta, and H. Iyetomi: Solid State Commun. **151** (2011) 1605.
14) JEITA Standard eM-3508 (2005).
15) B.-S. Moon, B.-C. Sim, and J.-G. Park: Jpn. J. Appl. Phys. **49** (2010) 121301.
16) V. V. Voronkov: J. Cryst. Growth **59** (1982) 625.
17) V. V. Voronkov and R. Falster: J. Cryst. Growth **194** (1998) 76.
18) M. Akatsuka, M. Okui, S. Umeno, and K. Sueoka: J. Electrochem. Soc. **150** (2003) G587.
19) K. Nakamura, S. Maeda, S. Togawa, T. Saishoji, and J. Tomioka: in *High Purity Silicon VI*, ed. C. L. Claeys, P. Rai-Choudhury, M. M. Watanabe, P. Stalhofer, and H. J. Dawson (ECS, Pennington, NJ, 2000) Vol. PV2000-17, p. 31.
20) Y. Yamakawa, K. Mitsumoto, and Y. Ōno: *Proc. Int. Conf. New Quantum Phenomena in Skutterudite and Related Systems (Skutterudite 2007)*, J. Phys. Soc. Jpn. **77** (2008) Suppl. A, p. 266.
21) V. Dohm and P. Fulde: Z. Phys. B **21** (1975) 369.
22) B. Lüthi: *Physical Acoustics in the Solid State* (Springer, Heidelberg, 2005) Chap. 5, p. 67.
23) Y. Kuramoto, H. Kusunose, and A. Kiss: J. Phys. Soc. Jpn. **78** (2009) 072001.
24) R. Shiina, H. Shiba, and P. Thalmeier: J. Phys. Soc. Jpn. **66** (1997) 1741.
25) S. Nakamura, T. Goto, S. Kunii, K. Iwashita, and A. Tamaki: J. Phys. Soc. Jpn. **63** (1994) 623.
26) Y. Nemoto, T. Yamaguchi, T. Horino, M. Akatsu, T. Yanagisawa, T. Goto, O. Suzuki, A. Dönni, and T. Komatsubara: Phys. Rev. B **68** (2003) 184109.
27) B. Bleaney and K. W. H. Stevens: Rep. Prog. Phys. **16** (1953) 108.
28) G. H. Dieke and H. M. Crosswhite: Appl. Opt. **2** (1963) 675.
29) G. D. Watkins: in *Deep Centers in Semiconductors*, ed. S. T. Pantelides (Gordon and Breach, New York, 1992) 2nd ed., Chap. 3, p. 177.
30) M. Lannoo, G. A. Baraff, and M. Schlüter: Phys. Rev. B **24** (1981) 955.
31) T. Hotta: Phys. Rev. Lett. **96** (2006) 197201.
32) K. Araki, T. Goto, K. Mitsumoto, Y. Nemoto, M. Akatsu, H. S. Suzuki, H. Tanida, S. Takagi, S. Yasin, S. Zherlitsyn, and J. Wosnitza: J. Phys. Soc. Jpn. **81** (2012) 023710.
33) K. Wilson: Rev. Mod. Phys. **47** (1975) 773.
34) K. Yosida: Phys. Rev. **147** (1966) 223.

©2013 The Physical Society of Japan